Design and Analysis of a Broadband Microwave Metamaterial Absorber

Yufei Zhang ⬤, Wenrong Yang ⬤, Xiaonan Li ⬤, and Guoqiang Liu ⬤

Abstract—In this article, a broadband metamaterial absorber suitable for the S, C, and X bands is designed and manufactured. The absorber is made of FR-4 substrate, resonant metal structure, lumped resistance, and metal backplate, has a unit size of $0.11\lambda_L$, and a total thickness of $0.084\lambda_L$. The absorption principle of the absorber is analyzed using equivalent medium theory and parametric research. The calculation results show that the absorber achieves more than 90% broadband absorption (relative bandwidth of 130%) between 2.7 GHz and 12.7 GHz, has a good polarization angle and incidence angle insensitivity, uses electromagnetic resonance to explain its absorption characteristics, and experiments confirm that the absorber has good broadband absorption. The proposed absorber has higher absorption and simpler construction than the previously described broadband absorber, and it has the potential for practical applications in EMC, radar, and electromagnetic protection.

Index Terms—Metamaterial, broadband, microwave.

I. INTRODUCTION

METAMATERIALS are artificial composite structures or composite materials. By designing the unit's resonant characteristics, the equivalent electromagnetic parameters of the material can be effectively controlled in a given frequency band. In stealth cloaks [1], [2], microwave filters [3], [4], antenna design [5], [6], wavefront manipulation [7], [8], [9], [10], solar converters [11], tunable meta-surface [12] and other technologies, metamaterials have achieved great advances. A metal structure known as a metamaterial absorber restricts electromagnetic (EM) waves by reflection and transmission [13]. Landy and Smith introduced the idea of a Perfect Metamaterial Absorber in 2008. (PMA). It's narrow-band performance and polarization sensitivity constrain the range of applications for PMA [14]. PMA is based on the resonant characteristics of the unit to achieve perfect absorption, the design structure generates resonance at specific frequency points, and the incident electromagnetic wave is converted into other forms of energy. Later, various single-frequency or multi-frequency polarization-insensitive absorbers were proposed in the study [15], [16], [17], [18], [19], [20].

Metamaterial absorbers (MA) have made significant progress in the past decade. However, due to the limitations of the natural resonance of MA, its bandwidth is difficult to widen, so many methods for widening the MAs band have been proposed. The first method commonly used to enhance bandwidth is a single-layer absorber structure, which consists of resonant elements with different geometric parameters [21], [22], [23], superimposing the resonance points of different sizes of resonant elements to increase the overall bandwidth. Another method is multi-layer construction [24], [25], [26], [27], [28], due to the absorbing layer's large unit volume and processing complexity, these methods have certain limitations in practical applications. In recent years, symmetrical structures based on lumped elements can be considered an emerging and promising alternative to designing broadband absorbers with sufficiently large bandwidth, high efficiency, and polarization insensitivity [29], [30], [31], [32]. Fan designed a metamaterial absorber with an angle-insensitive angle in the 3-10GHz wide band. Its structure uses eight lumped resistors and air layer to achieve broadband absorption [33]. Thi Kim Thu Nguyen designed a simple structure absorber, using a simple design of the fractal structure and loading lumped resistors to achieve the effect of covering both the X-band and the Ku-band [34]. Awanish Kumar designed a metamaterial absorber consisting of a crossed arrow resonator and four SMD resistors to achieve high absorption covering the C-band and X-band, with near-perfect absorption in some frequency bands [35].

A new broadband metamaterial absorber with polarization and incidence angle insensitivity is proposed in this work. Designing resonant units filled with lumped resistors results in broadband absorption in the S, C, and X bands. The surface current density, electric field distribution, and input impedance characteristics of the unit are analyzed using CST MICROWAVE STUDIO2019 simulation software, and the wave absorption mechanism of the proposed structure is explained. Finally, the absorber was manufactured and tested to ensure the design could meet the absorption application in the target frequency band.

II. TRANSMISSION LINE THEORY AND EQUIVALENT MEDIA THEORY

The characteristics of the absorber are related to the degree of impedance matching, as shown in Fig. 1, and the absorption phenomenon can be understood through a transmission line model [20]. The end of the transmission line is a copper backplane, equivalent to a short circuit. The h_1 part of the transmission line represents the air layer. In contrast, the h_2 section of the
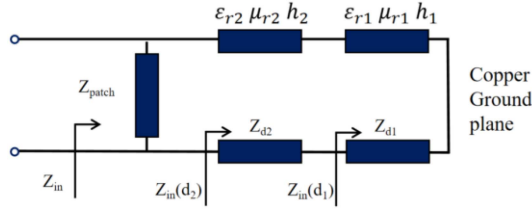
Fig. 1.   Equivalent transmission line model of the proposed absorber.

transmission line describes the FR-4 dielectric substrate, and the Z_{patch} represents the resonant metal structure on the surface of the circuit.

$$Z_{in}(d_1) = jZ_{d1} \tan \beta_1 h_1 = jZ_0 \sqrt{\frac{\mu_{r1}}{\varepsilon_{r1}}} \tan \frac{2\pi h_1 \sqrt{\mu_{r1}\varepsilon_{r1}}}{\lambda} \tag{1}$$

$$Z_{in}(d_2) = Z_{d2} \frac{Z_{in}(d_1) + jZ_{d2} \tan \beta_2 h_2}{Z_{d2} + jZ_{in}(d_1) \tan \beta_2 h_2} \tag{2}$$

$$\Gamma = \frac{Z_{patch} || Z_{in}(d_2) - Z_0}{Z_{patch} || Z_{in}(d_2) + Z_0} \tag{3}$$

Where $\beta_1 = 2\pi \sqrt{\mu_{r1}\varepsilon_{r1}}/\lambda$. $Z_{in}(d1)$ represents the input impedance of the air layer, $Z_{in}(d2)$ represents the combined input impedance of FR-4 and the air layer, and Γ represents the input impedance of the overall absorption unit. It can be seen from (3) that when the impedance is equal to the wave impedance in the air, the absorber will match the free space.

If the absorber is considered a homogeneous medium, the absorption rate can be expressed by (4), where S_{11} and S_{21} are the reflection coefficient and transmission coefficient of the absorber. Correspondingly, R and T are the reflectivity and transmittance. To prevent electromagnetic wave transmission, we add a metal plate to the absorber's bottom layer, making the transmission coefficient S_{21} tend to zero. And to obtain the maximum absorption rate at a particular frequency point, the value of the reflection coefficient S_{11} should be 0.

$$A(\omega) = 1 - |S_{11}(\omega)|^2 - |S_{21}(\omega)|^2 = 1 - R - T \tag{4}$$

Assuming that the electromagnetic wave is incident vertically on a structure of thickness d, its refractive index n and normalized impedance z can be expressed as (5) and (6):

$$n = \frac{1}{kd} \cos^{-1} \left[\frac{1}{S_{21}} (1 - S_{11}^2 + S_{21}^2) \right] \tag{5}$$

$$z = \sqrt{\frac{(1 + S_{11})^2 - S_{21}^2}{(1 - S_{11})^2 + S_{21}^2}} \tag{6}$$

The relative permittivity of the absorber can be calculated as $\varepsilon_{eff} = n/z$, the relative permeability can be calculated as $\mu_{eff} = nz$, and the reflection and transmission coefficients can be used to calculate the absorber's relative permittivity and permeability.
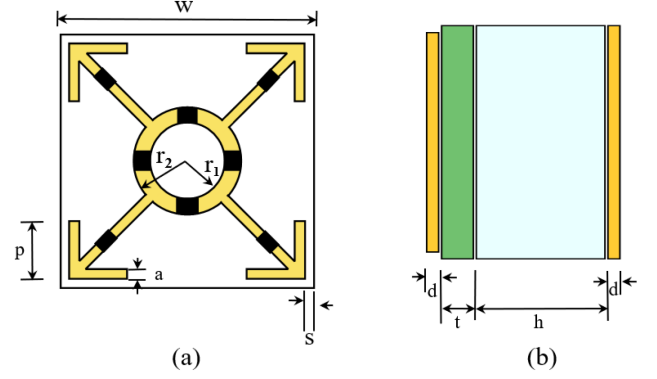

(a)   (b)

(c)

Fig. 2.   Schematic of the proposed wideband unit (a) top view (b) left view (c) schematic illustration of the absorber.

III.   SIMULATION AND DESIGN OF BROADBAND METAMATERIAL ABSORBER

The design unit consists of three layers: a dielectric substrate printed with a metal resonance layer, an air layer, and a metal copper plate, as shown in Fig. 2(a) and (b). The top layer consists of a ring and four arrows and is loaded with eight lumped resistors; the resistance near the ring is named R1, and the resistance near the arrow is R2 (R1 = 110 Ω, R2 = 120 Ω). The dielectric substrate is made of FR-4 with a thickness of 0.2 mm, where the relative permittivity of FR-4 is 4.3, and the loss tangent is 0.025. Between the top and bottom metal plates is an air layer with a height of 9 mm. The top resonant ring and the underlying metal are made of copper (5.96 × 10⁷ S/m) with a thickness of 0.035 mm. The element size is 12 mm × 12 mm, the offset distance between the arrow and the element s = 0.2 mm, the arrow edge length p = 3 mm, and the inner and outer diameters of the ring are 2 mm and 2.7 mm, respectively. All parameters are shown in Table I.

For simulations, the frequency domain solver of the commercial simulation software CST is used to optimize the geometric parameters of the absorber several times. The simulation adopts unit cell condition in the x and y directions and open (add space) in the z-direction, and the incident wave is polarized in the z-direction. Except for the polarization and incidence analyses,

TABLE I
LIST OF PARAMETERS OF THE PROPOSED WIDEBAND UNIT

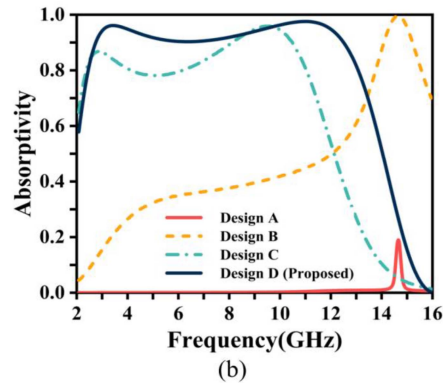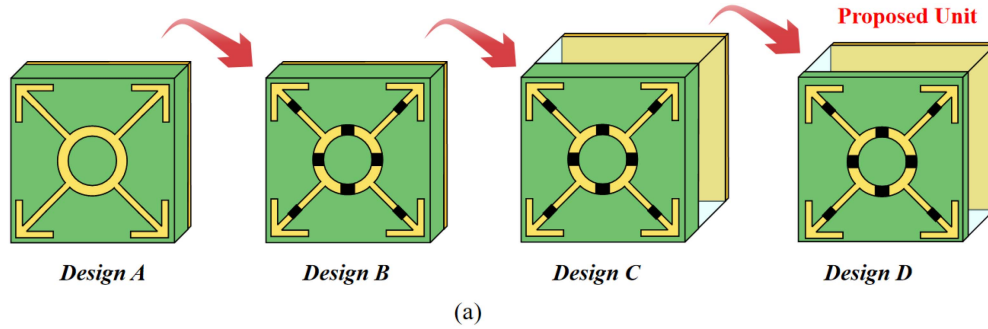| Parameter	r_1	r_2	w	s	p	a	t	h	d
Value(mm)	2	2.7	12	0.2	3	0.5	0.2	9	0.035

(a)

(b)

Fig. 3. (a) Different design step of the proposed wideband unit; (b) the simulated absorptivity response of different design steps.

all variables are only simulated by TE wave. The schematic diagram of the absorber is shown in Fig. 2(c)

A. The Design Concept Evaluations

The design process of the broadband absorber is divided into four steps, as shown in Fig. 3(a). The design of the model initially originated from Design A. The thickness of the dielectric substrate FR-4 of Design A is 2 mm, and the resonant pattern of the top layer of the dielectric substrate is designed with a fractal geometry, which is intended to make the absorber insensitive to electromagnetic wave polarization. The absorptivity curve is shown in Fig. 3(b). The absorbance of the design unit is only 20% at 14.7 GHz when the loss of the incident electromagnetic wave is mainly the dielectric loss of the material itself. In order to broaden the absorption bandwidth of the absorber model, eight lumped resistors are added to increase the absorption bandwidth as Design B achieves more than 90% absorption at 14–15 GHz, with a perfect absorption of more than 99% at 14.6 GHz, but still fails to provide a broader absorption in the target range. To further broaden the absorption

bandwidth, the overall relative permittivity of the absorbing model was reduced by adding an air layer between the metal backplane and the dielectric substrate. It can be observed that there is already a significant band-broadening effect in Design C compared to Structure Design A and Structure Design B, but it still needs to meet the design goal of covering the S, C, and X bands. Finally, by modifying the resistive resistance and dielectric substrate height, Design D achieves more than 90% absorption from 2.7 GHz to 12.7 GHz with a relative absorption bandwidth of 130%, virtually completely covering the S, C, and X bands.

Fig. 4(a) shows the normalized impedance of the absorber. The real part of the normalized impedance tends to be one, and the imaginary part is approximately 0 at 2.7–12.7 GHz, which indicates that the absorber has an excellent overall match with the wave impedance of space in this frequency range.

Fig. 4(b) depicts the relative permittivity and permeability of the absorber. The lossy impact of electromagnetic waves is provided by the imaginary component of the relative permittivity $\mathrm{Im}(\varepsilon)$ and the imaginary part of the relative permeability $\mathrm{Im}(\mu)$. At the same time, there are some discrepancies in the real parts of
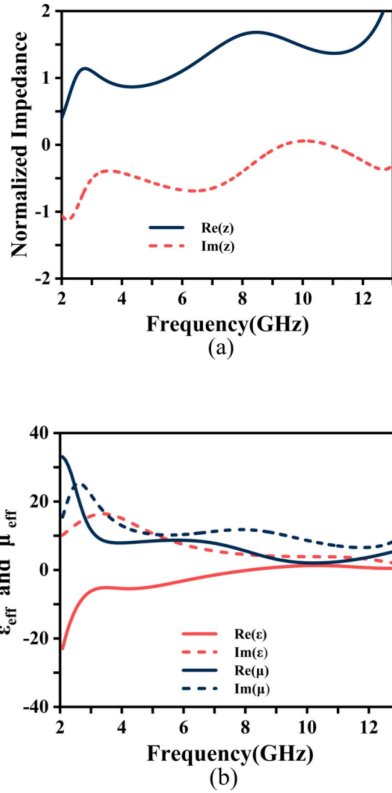
Fig. 4. (a) Simulated normalized impedance of the proposed wideband unit; (b) simulated relative permittivity and relative permeability of the proposed wideband unit.
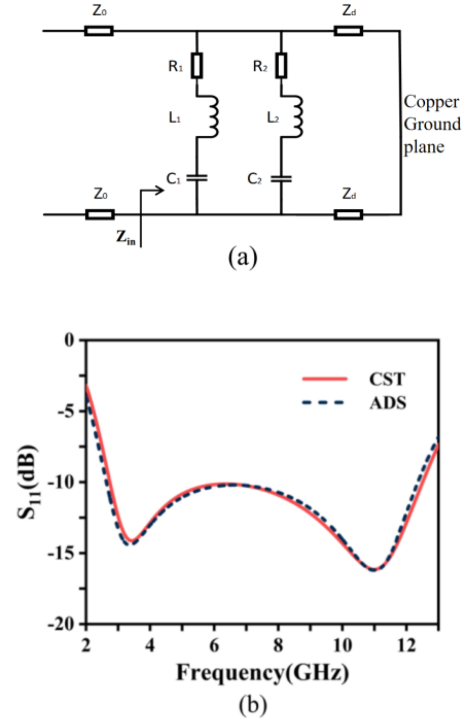

Fig. 5. (a) Equivalent circuit model of the proposed wideband unit; (b) S_{11} comparison between the numerical simulation (CST) and circuit simulation (ADS).
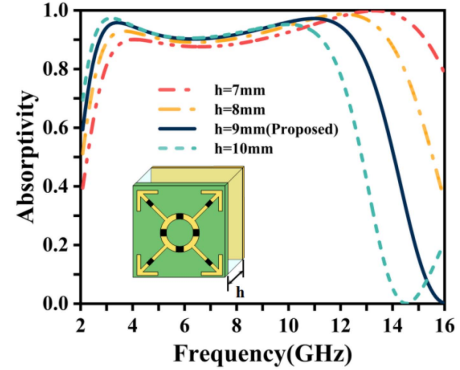

Fig. 6. Simulated absorptivity of the wideband unit varies with the height of the air layer.

the relative permittivity $Re(\varepsilon)$ and relative permeability $Re(\mu)$, which is why the design model is difficult to accomplish perfect absorption in the target band.

To better understand the absorption mechanism of this designed unit, an equivalent circuit is built for analysis. The Z_{patch} is evaluated as two parallel R-L-C resonant circuits corresponding to two neighboring superimposed resonant peaks in the absorption band, as shown in Fig. 5(a). The ADS extracted and calculated parameter values for the absorber concentrating elements are $R_1 = 222$, $R_2 = 70$, $L_1 = 3.255$ nH, $L_2 = 5.481$ nH, $C_1 = 0.2358$ pF, $C_2 = 21.052$ fF. The S_{11} parameters acquired by ADS and CST were then compared and found to be almost identical for both curves.

B. The Effect of Changing Air Thickness

It is crucial to investigate the relationship between dielectric layer thickness and absorption rate. According to transmission line theory, changing the dielectric layer thickness will change the input impedance of the cell and thus affect the absorption rate. Fig. 6 depicts the absorbance at different air layer heights. Keeping the other parameters as shown in Table I and increasing only the height of the air layer, it can be seen that the second absorption peak gradually approaches the lower frequencies. To cover the S, C and X bands, h = 9 mm was utilized as the optimized value.

Fig. 7 illustrates how absorptivity is affected by various FR-4 layer thicknesses. The second absorption peak gradually narrows and shifts to a low frequency as the dielectric substrate layer's thickness rises. It seems that a thin dielectric substrate layer would produce a broad absorption band; however, t = 0.2 mm was chosen as the optimization value for the S, C, and X bands because a thin dielectric substrate layer poses some challenges in both physical manufacture and application.

C. The Effect of Changing Outer and Inner Diameters

The inner and outer diameters of the circular ring are two characteristics that must be considered for our design. The radius
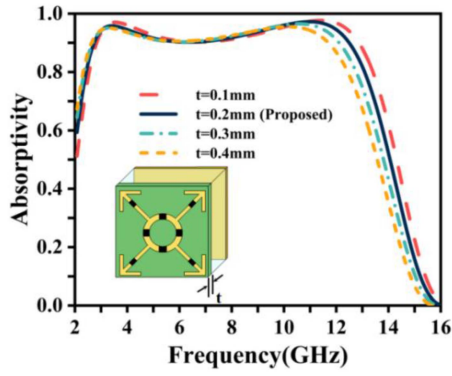
Fig. 7. Simulated absorptivity of the wideband unit varies with the height of the air layer.
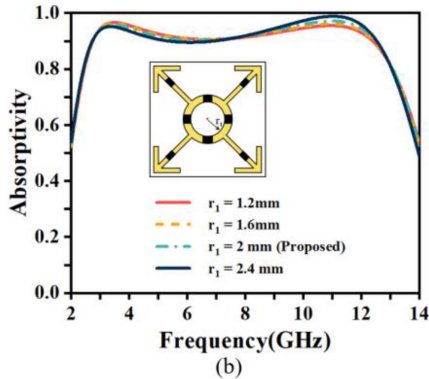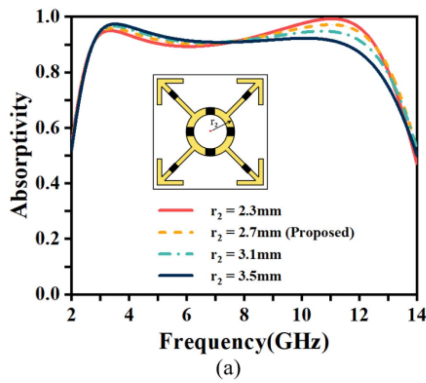

Fig. 8. Simulated absorptivity of the wideband unit varies with the r_2 (a) and r_1 (b).

Fig. 9. (a) Simulated S_{11} of the wideband unit varies with the spacing s. (b) Simulated absorptivity of the wideband unit varies with the arrow's edge length p.

is exactly opposite to the trend of the outer diameter r_2. After optimising the model calculation, we determined $r_1 = 2$ mm, and $r_2 = 2.7$ mm as the suit values.

D. The Effect of Spacing and Edge Length of Arrows

The spacing between units and arrows is an essential parameter, thus S_{11} was chosen to reflect the discrepancy with the control group, as shown in Fig. 9(a).

Keeping the other parameters in Table I constant, the number of absorption peaks is closely related to the variation of the spacing s. When s gradually decreases, a new resonant peak appears in the absorption band near the high-frequency band due to the equivalent capacitance between the arrows of the periodic array unit under the action of the electric field. As the spacing increases, the equivalent capacitance between units changes, the absorption summit near the high-frequency band gradually flattens, and the overall absorption bandwidth decreases. To meet the wider absorption band, s = 0.2 mm is selected as the spacing between the cell boundary and the arrow for this broadband design.

Meanwhile, the edge length of the arrow is also one of the critical parameters affecting the absorption rate, as shown in Fig. 9(b). As the edge length p increases, the absorption peak

size must be selected to ensure good absorption in the intended frequency band and allow for easy surface resistance installation. Fig. 8(a) and (b) show the effect of adjusting the inner diameter r_2 and outer diameter r_1 on the absorption rate.

When the inner diameter of the ring $r_1 = 2$ mm and the outer diameter r_2 is continuously increased from 2.3 mm, the absorption at around 4 GHz gradually increases, while the absorption peak at approximately 11 GHz gradually decreases from nearly 100% to 90%. But when the circle $r_2 = 2.7$ mm is constant, and the inner diameter is continuously increased from 1.2 mm, the absorption peak at 4 GHz gradually decreases while the absorption peak at 11 GHz constantly increases, which
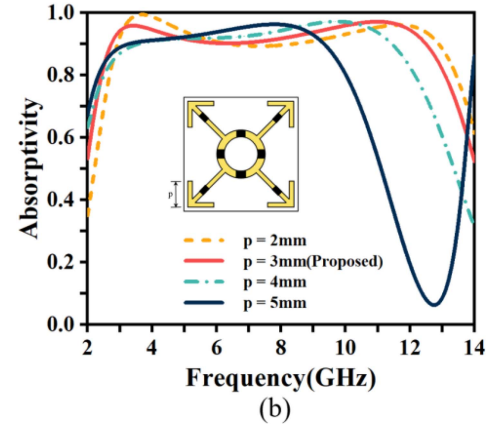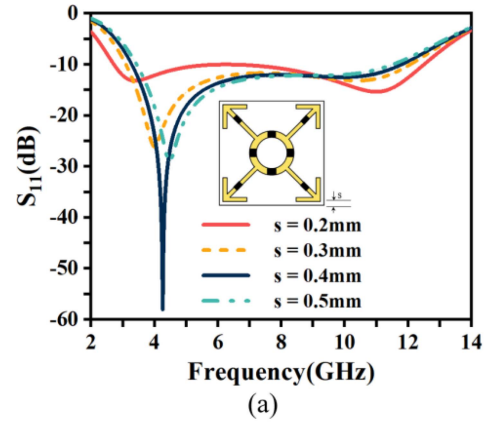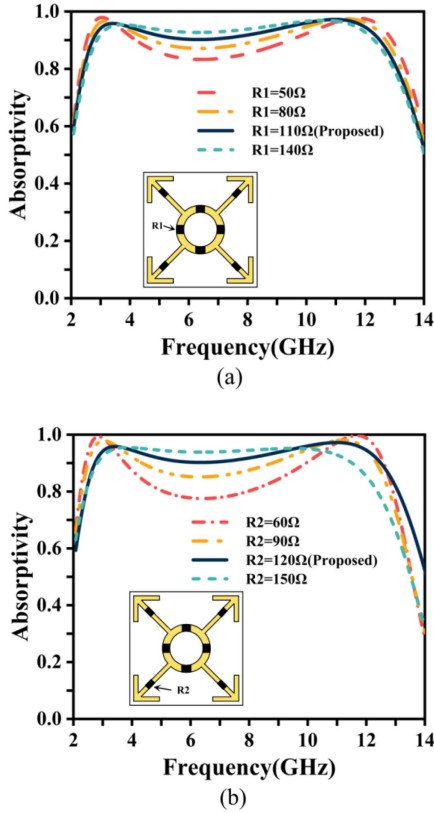
Fig. 10.   (a) Simulated absorptivity of the wideband unit varies with R1; (b) simulated absorptivity of the wideband unit varies with R2.

Fig. 11.   The simulated absorptivity at different angles for TE polarization (a) and TM polarization (b).

at high frequencies starts to approach low frequencies, which shortens the overall absorption bandwidth; while the absorption peak at low frequencies gradually shrinks, and when p increases to 5 mm, it can no longer meet the effective absorption at the low-frequency end. To produce an effective broadband absorption at the target 2-12 GHz, p = 3 mm is used as the parameter value for the design unit.

E. The Effect of Changing Lumped Resistors on Absorptivity

Keep the other parameters in Table I unchanged, Fig. 10(a) displays the change in absorption rate as a function of R1; for R1 = 50 Ω, the absorption curve exhibits significant absorptivity at both 3.4 GHz and 11 GHz, whereas the absorption effect in the middle band is less than 90%. The absorption curve's bandwidth considerably increases as R1 resistance is raised. When R1 = 140 Ω, the peak at both ends of the absorption curve decreases and the entire absorption bandwidth begins to shrink.

Fig. 10(b) illustrates how the absorption rate changes as R2 changes. When R2 = 60 Ω, the absorption curve yields perfect absorption peaks at 3.4 GHz and 11 GHz. The absorption peaks on both sides of the curve gradually flattened with increased R2, and the absorption bandwidth got better. The total absorption bandwidth starts to decrease when R2 reaches 150 Ω. After continuous calculation and optimization, both R1 = 110 Ω and R2 = 120 Ω were selected as the resistors of the design unit.
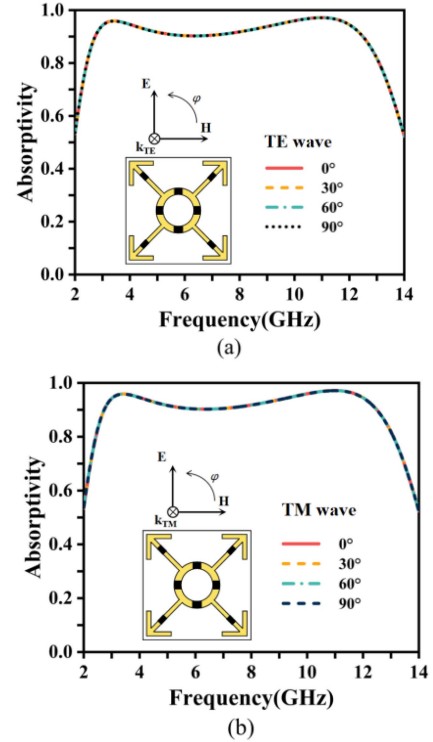
F. Effect of Polarization and Incidence Angle

Maintaining a wide incidence and polarization angle absorption response is an essential factor in designing a metamaterial absorber; the absorption characteristics at different polarization angles of incidence in TE and TM modes are shown in Fig. 11(a) and (b). In TE mode, the z-axis is the propagation direction of the wave vector, and the electric field vector (Ex) and the magnetic field vector (Hy) propagate along the x-axis and y-axis, respectively. In contrast, the magnetic field vector has a component (Hz) along the z-axis. In TM mode, the electric field vector has components (Ez) in the direction of the z-axis, and the magnetic field (Hx) and electric field (Ey) vectors along the x-axis and y-axis, respectively [36]. Since the proposed absorber structure has good axial symmetry, the absorption curve of the unit hardly changes with the adjustment of polarization incidence angle, indicating that the structure has good polarization incidence insensitivity characteristics.

Fig. 12(a) and (b), correspondingly, display the absorption properties in the TE and TM modes at the angle of incidence. In TE mode, as the incidence angle increases, the second peak of the absorption curve shifts to the high-frequency band and, at some frequency points, even achieves a perfect absorption effect of more than 99%. When the incidence angle is increased to 20°, the absorber can still guarantee an absorption rate of more than 90% at frequencies between 2.7 and 12.7 GHz. It can also still guarantee an absorption rate of more than 80% at these same frequencies when the incidence angle is increased to 40°. In TM mode, the absorption effect between 2.7 GHz and
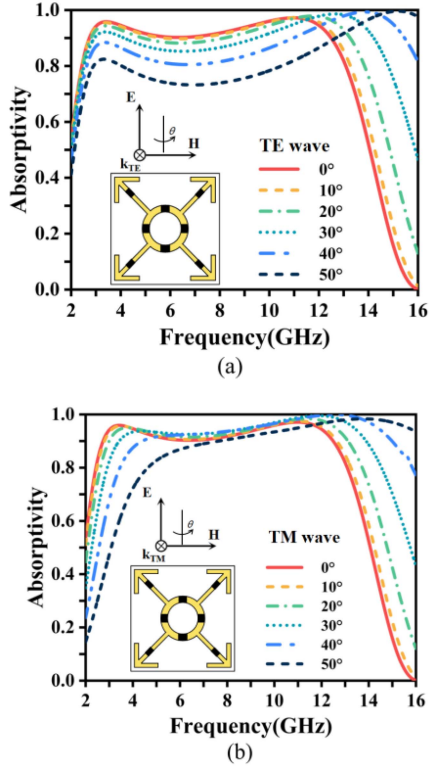
Fig. 12. The simulated absorptivity at different incident angles for TE wave (a) and TM wave(b).

12.7 GHz changes less when the angle of incidence is increased to 20°. Even when the angle of incidence is increased to 40°, the majority of the target frequency bands can still achieve an absorption effect of more than 80%. These results indicate that the designed unit has the characteristic of wide incidence angle absorption.

G. Analysis of Absorption Mechanism

We simulated the absorber's surface electric field and surface current distribution at 3.4 GHz and 11 GHz under TE wave excitation in the XOY plane in order to further investigate the absorption mechanism of this design unit. The distribution of absolute of the surface E-field ($|E|$) is shown in Fig. 13(a) and (d). At either 3.4 GHz or 11 GHz, the electric field is mainly distributed where the lumped resistance is loaded and in the boundary region. The lump resistors on the diagonal can collect electric field under the TE wave. However, the highest level of the electric field at the circle is mostly distributed on the left and right sides, which is related to the polarization angle of the TE wave. Since the absorber is a periodic unit array structure, the equivalent capacitance can be formed between adjacent structures, and the E-field also appears as a maximum at the upper and lower boundaries, which contributes to the formation of electric coupling.

The surface current distribution at 3.4 GHz is depicted in Fig. 13(b) and (c); the top surface current is parallel to the bottom surface current in the opposite direction, and the upper and lower

sides form a cyclic current loop, indicating that the field coupling is formed in a closed loop and that the magnetic resonance is related to this resonant frequency. At the resonant frequency of 11 GHz, the surface current is parallel to the direction of the bottom current, as shown in Fig. 13(e) and (f). The surface current flows in the opposite direction of the electric field provided by the incident TE wave, showing that electrical resonance is the dominant resonance mode at this resonant frequency. At two resonant frequencies, the current intensity in the bottom layer is much lower than in the top layer, indicating that the majority of the electromagnetic energy is dissipated in the top layer, and the ohmic loss provides effective broadband absorption for this absorbing structure.

IV. EXPERIMENT AND DISCUSSION

Fig. 14(b) depicts a sample printed copper structure with a thickness of 0.2 mm on a FR-4 surface with dimensions of 24 cm × 24 cm. The two resistors, R1 = 110 Ω and R2 = 120 Ω, are 0402 chip resistors, and a foam strip is utilized to support the four sides of the absorber, resulting in a 9 mm high air layer. We put the horn antenna (transmitter and receiver) through its paces in Horizontal and vertical polarization at four different frequencies: 2 to 4 GHz, 4 to 8 GHz, 8 to 12 GHz, and 12 to 18 GHz, as illustrated in Fig. 14(a).

A wideband absorber's reflection coefficient S_{11} was determined using the bow method; Fig. 14(c) displays the observed S_{11} characteristics, it is clear that the experiment only achieves a resonance peak at 4.2 GHz, which deviates slightly from the simulation data but still results in an absorption rate of more than 90% at 3 GHz to 11 GHz, with the perfect absorption of more than 99% achieved at 4–5.2 GHz. The relative bandwidth of the overall absorption reaches 114%, which still satisfies the broadband absorption effect of the target design band.

Additionally, we discovered that when the element boundary and arrow spacing parameter values were changed to s = 0.4 mm, the simulated reflection parameter curve only had one perfect absorption peak and satisfied the broadband absorption, closely matching the experimentally measured reflection parameter curve shown in Fig. 14(d). As mentioned, the element boundary and arrow spacing (s) are crucial factors in producing absorption peaks, demonstrating that the difference between the experiment and the computation is caused mostly by a lack of machining accuracy.

Fig. 14(e) and (f) show S_{11} data for TE and TM modes from various angles. Under TE wave incidence, the incidence angle of 4° produces a perfect absorption peak at 4.2 GHz, which nearly meets more than 90% of the effective absorption in the 2–12 GHz band. When the incidence angle increases to 30°, the absorption near the 8 GHz band decreases to less than 90% but still almost meets about 90% absorption in the entire target band. Similarly, the TM wave incident at an incidence angle of 4° also meets the effective broadband absorption in the 2–12 GHz band. Still, unlike the TE wave, when the incidence angle is increased to 30°, two resonance peaks appear between 5 GHz and 12 GHz and form nearly 99% of the broadband absorption, but the absorption
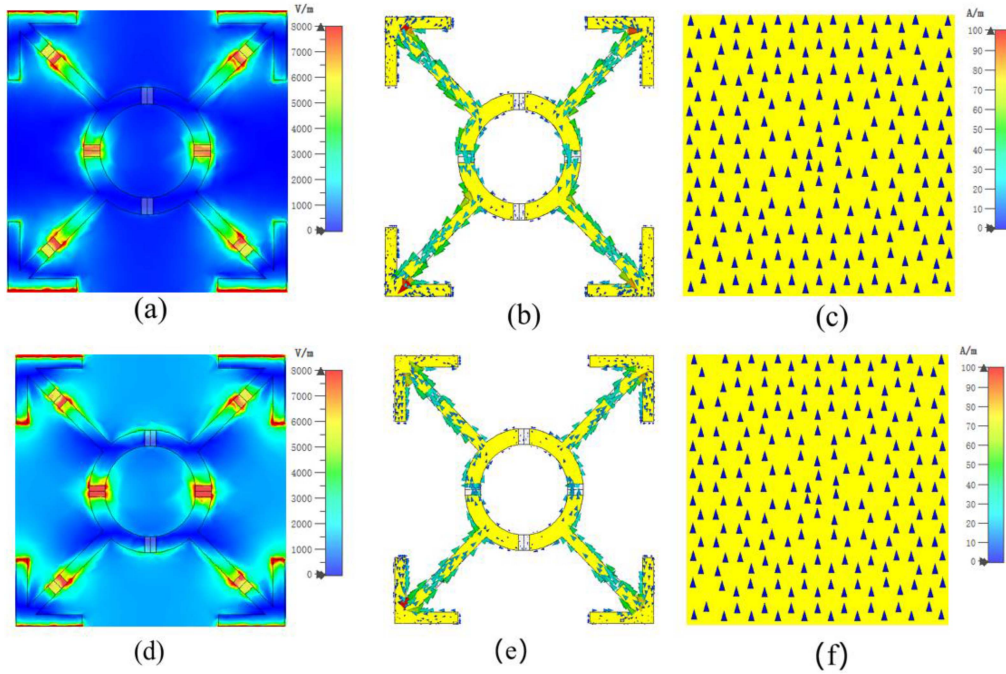
Fig. 13.   Electric field distribution on the top layer of the wideband unit at 3.4 GHz (a) and 11 GHz (b); surface current distribution at 3.4 GHz (b) and 11 GHz (e); bottom current distribution at 3.4 GHz (c) and 11 GHz (f).
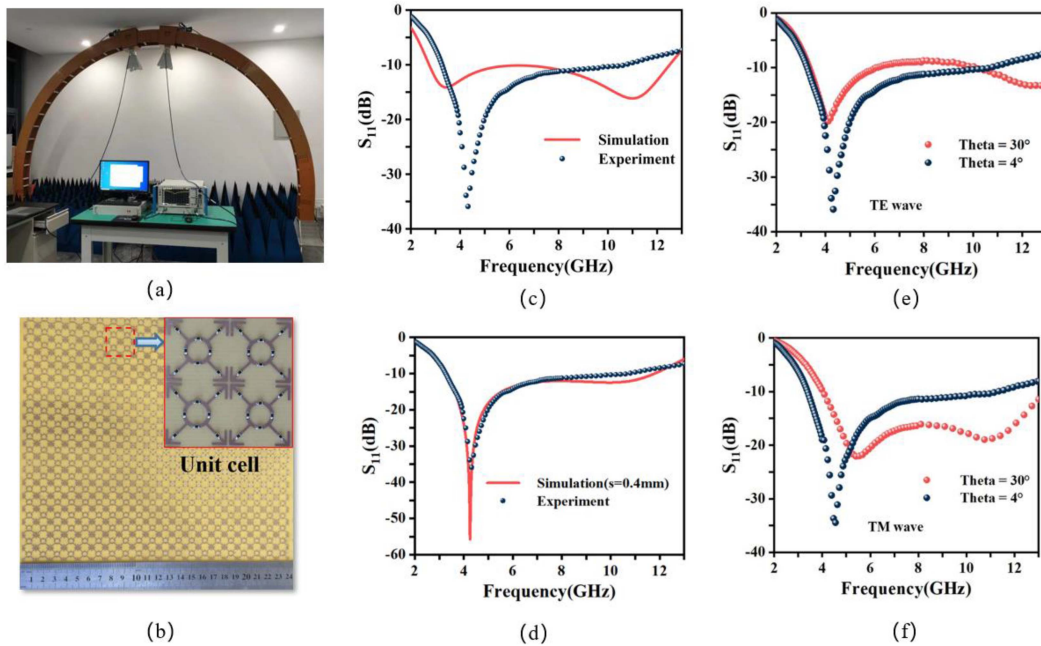

Fig. 14.   (a) Experimental test platform; (b) photograph of the fabricated absorber; (c) comparison of experiment and simulation of S_{11}; (d) comparison of experiment and simulation of S_{11} (s = 0.4 mm); (e) the measured S_{11} of the absorber under incident angles of 4°and 30°at TE wave; (f) the measured S_{11} of the absorber under incident angles of 4°and 30°at TM wave.

band is shortened and shifted. Despite the deviation of the experimental results from the simulated calculations, our designed absorber still has the capability of wide-angle incidence.

Comparisons are made between the suggested absorber structure and previously published structures, as shown in Table II.

The benefit of the suggested structure is its simple structural design, which not only results in a small electrical size and thickness of the unit but also a broad absorption band with a calculated relative bandwidth of 130%, nearly covering the S, C, and X bands. The proposed structure is also insensitive to

TABLE II
COMPARISON OF PROPOSED WORK WITH PREVIOUS WIDEBAND ABSORBERS

References	Working frequency (GHz)	RBW (%)	Unit cell size	Thickness	polarization Insensitivity	Unit Cell Properties
[33]	2.5-10.1	119%	$0.16\lambda_L$	$0.083\lambda_L$	Yes	1 sheet + air gap +8 resisters
[34]	8-18	77%	$0.26\lambda_L$	$0.067\lambda_L$	Yes	1 sheet + 4 resisters
[37]	7.6-18.3	83%	$0.26\lambda_L$	$0.083\lambda_L$	Yes	1 sheet + silicon rubber + 4 resisters
[38]	4.3-11.1	88%	$0.172\lambda_L$	$0.138\lambda_L$	yes	4 sheets + 2 sheet resistances
[39]	8.9-14	44.5%	$0.28\lambda_L$	$0.03\lambda_L$	yes	PVC + OCA + PET + ITO resistive film
[40]	11.4-20	55%	$0.29\lambda_L$	$0.13\lambda_L$	No	1 sheet
Proposed	2.7-12.7	130%	$0.11\lambda_L$	$0.084\lambda_L$	Yes	1 sheet + air gap +8 resisters

where λ_L is the wavelength corresponding to the lowest absorption frequency;

RBW = $2*((f_{max}-f_{min})/(f_{max}+f_{min}))*100\%$

polarization and incidence angle, enabling it to realize wide-band absorption in the microwave band.

V. CONCLUSION

This study proposes a broadband metamaterial absorber that operating in the S, C, and X bands. The unit use a resonant metal structure with eight chip resistors, combined with FR-4 dielectric substrate and air layer, and was able to absorb electromagnetic waves in the 2.7–12.7 GHz band and achieve more than 90% absorptivity. Theoretical analysis of the absorber showed that the absorber is insensitive to electromagnetic waves in both TE and TM modes and can maintain an absorption rate of more than 80% at an incidence angle of less than 40°. Finally, the experimental measurement of the reflection coefficient S_{11} reveals a correspondence between the physical and simulated absorption characteristics. These outcomes demonstrate the proposed absorber's suitability for EMC, radar, and electromagnetic protection applications.

REFERENCES

[1] D. Schurig et al., "Metamaterial electromagnetic cloak at microwave frequencies," *Science*, vol. 314, no. 5801, pp. 977–980, Nov. 2006.

[2] J. B. Pendry, D. Schurig, and D. R. Smith, "Controlling electromagnetic fields," *Science*, vol. 312, no. 5781, pp. 1780–1782, Jun. 2006.

[3] H. Lobato-Morales, A. Corona-Chavez, and J. Rodriguez-Asomoza, "Microwave directional filters using metamaterial closed-loop resonators," *Microw. Opt. Technol. Lett.*, vol. 51, no. 5, pp. 1155–1156, May 2009.

[4] I. B. Vendik and O. G. Vendik, "Metamaterials and their application in microwaves: A review," *Tech. Phys.*, vol. 58, no. 1, pp. 1–24, Jan. 2013.

[5] J. Ren, S. Gong, and W. Jiang, "Low-RCS monopolar patch antenna based on a dual-ring metamaterial absorber," *IEEE Antennas Wireless Propag. Lett.*, vol. 17, no. 1, pp. 102–105, Jan. 2018.

[6] S. Enoch, G. Tayeb, P. Sabouroux, N. Guerin, and P. Vincent, "A metamaterial for directive emission," *Phys. Rev. Lett.*, vol. 89, no. 21, Nov. 2002, Art. no. 213902.

[7] C. Wang et al., "Heterogeneous Amplitude−Phase metasurface for distinct wavefront manipulation," *Adv. Photon. Res.*, vol. 2, no. 10, Oct. 2021, Art. no. 2100102.

[8] M. Euler, V. Fusco, R. Dickie, R. Cahill, and J. Verheggen, "Sub-mm wet etched linear to circular polarization FSS based polarization converters," *IEEE Trans. Antennas Propag.*, vol. 59, no. 8, pp. 3103–3106, Aug. 2011.

[9] B. Lin, L. Lv, J. Guo, Z. Liu, X. Ji, and J. Wu, "An ultra-wideband reflective linear-to-circular polarization converter based on anisotropic metasurface," *IEEE Access*, vol. 8, pp. 82732–82740, 2020.

[10] T. K. T. Nguyen et al., "Simple design of efficient broadband multifunctional polarization converter for X-band applications," *Sci. Rep.*, vol. 11, no. 1, Jan. 2021, Art. no. 2032.

[11] L. Zhu, Y. Wang, Y. Liu, and C. Yue, "Design and analysis of ultra broadband nano-absorber for solar energy harvesting," *Plasmonics*, vol. 13, no. 2, pp. 475–481, Apr. 2018.

[12] H.-X. Xu et al., "Adaptable invisibility management using Kirigami-inspired transformable metamaterials," *Research*, vol. 2021, Sep. 2021, Art. no. 9806789.

[13] D. R. Smith, W. J. Padilla, D. C. Vier, S. C. Nemat-Nasser, and S. Schultz, "Composite medium with simultaneously negative permeability and permittivity," *Phys. Rev. Lett.*, vol. 84, no. 18, pp. 4184–4187, May 2000.

[14] N. I. Landy, S. Sajuyigbe, J. J. Mock, D. R. Smith, and W. J. Padilla, "Perfect metamaterial absorber," *Phys. Rev. Lett.*, vol. 100, no. 20, May 2008, Art. no. 207402.

[15] J. Yang and Z. Shen, "A thin and broadband absorber using double-square loops," *IEEE Antennas Wireless Propag. Lett.*, vol. 6, pp. 388–391, Dec. 2007.

[16] S. Bhattacharyya, S. Ghosh, and K. V. Srivastava, "Triple band polarization-independent metamaterial absorber with bandwidth enhancement at X-band," *J. Appl. Phys.*, vol. 114, no. 9, Sep. 2013, Art. no. 094514.

[17] A. Kumar, J. Padhi, G. S. Reddy, and S. Narayan, "Dual band polarization insensitive frequency selective surface absorber," in *Proc. IEEE Microw. Theory Technol. Soc. Int. Microw. RF Conf.*, 2019, pp. 1–5.

[18] X. Shen, T. J. Cui, J. Zhao, H. F. Ma, W. X. Jiang, and H. Li, "Polarization-independent wide-angle triple-band metamaterial absorber," *Opt. Exp.*, vol. 19, no. 10, pp. 9401–9407, May 2011.

[19] H.-X. Xu, G.-M. Wang, M.-Q. Qi, J.-G. Liang, J.-Q. Gong, and Z.-M. Xu, "Triple-band polarization-insensitive wide-angle ultra-miniature metamaterial transmission line absorber," *Phys. Rev. B*, vol. 86, no. 20, Nov. 2012, Art. no. 205104.

[20] K. Li et al., "Multi-band polarization-insensitive metamaterial absorber for microwave based on slotted structure and magnetic rubber," *Polymers*, vol. 14, no. 8, Apr. 2022, Art. no. 1576.

[21] L. Li, Y. Yang, and C. Liang, "A wide-angle polarization-insensitive ultra-thin metamaterial absorber with three resonant modes," *J. Appl. Phys.*, vol. 110, no. 6, Sep. 2011, Art. no. 063702.

[22] S. Ghosh, S. Bhattacharyya, Y. Kaiprath, and K. V. Srivastava, "Bandwidth-enhanced polarization-insensitive microwave metamaterial absorber and its equivalent circuit model," *J. Appl. Phys.*, vol. 115, no. 10, Mar. 2014, Art. no. 104503.

[23] W. Ma, Y. Wen, and X. Yu, "Broadband metamaterial absorber at mid-infrared using multiplexed cross resonators," *Opt. Exp.*, vol. 21, no. 25, pp. 30724–30730, Dec. 2013.

[24] A. Dhumal, A. Bhardwaj, and K. V. Srivastava, "Polarization insensitive multilayered broadband absorber for L and S bands of the radar spectrum," *Microw. Opt. Technol. Lett.*, vol. 63, no. 4, pp. 1229–1235, Apr. 2021.

[25] F. Ding, Y. Cui, X. Ge, Y. Jin, and S. He, "Ultra-broadband microwave metamaterial absorber," *Appl. Phys. Lett.*, vol. 100, no. 10, Mar. 2012, Art. no. 103506.

[26] N. T. Q. Hoa, P. H. Lam, P. D. Tung, T. S. Tuan, and H. Nguyen, "Numerical study of a wide-angle and polarization-insensitive ultrabroadband metamaterial absorber in visible and near-infrared region," *IEEE Photon. J.*, vol. 11, no. 1, Feb. 2019, Art. no. 4600208.

[27] Y. K. Zhong, S. M. Fu, M.-H. Tu, B.-R. Chen, and A. Lin, "A multimetal broadband metamaterial perfect absorber with compact dimension," *IEEE Photon. J.*, vol. 8, no. 2, Apr. 2016, Art. no. 6801810.

[28] Y. Wang, H.-X. Xu, C. Wang, H. Luo, S. Wang, and M. Wang, "Multimode-assisted broadband impedance-gradient thin metamaterial absorber," *Adv. Photon. Res.*, vol. 3, no. 10, Oct. 2022, Art. no. 2200063.

[29] K. Chen, X. Luo, G. Ding, J. Zhao, Y. Feng, and T. Jiang, "Broadband microwave metamaterial absorber with lumped resistor loading," *EPJ Appl. Metamaterials*, vol. 6, pp. 1–7, 2019.

[30] Y. J. Kim et al., "Ultrathin microwave metamaterial absorber utilizing embedded resistors," *J. Phys. D-Appl. Phys.*, vol. 50, no. 40, Oct. 2017, Art. no. 405110.

[31] S. Li, J. Gao, X. Cao, W. Li, Z. Zhang, and D. Zhang, "Wideband, thin, and polarization-insensitive perfect absorber based the double octagonal rings metamaterials and lumped resistances," *J. Appl. Phys.*, vol. 116, no. 4, Jul. 2014, Art. no. 043710.

[32] T. Q. H. Nguyen, T. K. T. Nguyen, T. N. Cao, H. Nguyen, and L. G. Bach, "Numerical study of a broadband metamaterial absorber using a single split circle ring and lumped resistors for X-band applications," *Amer. Inst. Phys. Adv.*, vol. 10, no. 3, Mar. 2020, Art. no. 035326.

[33] S. Fan and Y. Song, "Ultra-wideband flexible absorber in microwave frequency band," *Materials*, vol. 13, no. 21, Nov. 2020, Art. no. 4883.

[34] T. K. T. Nguyen et al., "Simple design of a wideband and wide-angle insensitive metamaterial absorber using lumped resistors for X- and Ku-bands," *IEEE Photon. J.*, vol. 13, no. 3, Jun. 2021, Art. no. 2200410.

[35] A. Kumar, G. S. Reddy, G. Padhi, R. Jawale, and S. Narayan, "Wideband, polarization independent electromagnetic wave absorber using cross arrow resonator and lumped SMD resistors for C and X band applications," *Int. J. RF Microw. Comput.-Aid. Eng.*, vol. 32, no. 7, Jul. 2022, Art. no. e23163.

[36] M. L. Hakim et al., "Wide-oblique-incident-angle stable polarization-insensitive ultra-wideband metamaterial perfect absorber for visible optical wavelength applications," *Materials*, vol. 15, no. 6, Mar. 2022, Art. no. 2201.

[37] H. Chen et al., "Flexible and conformable broadband metamaterial absorber with wide-angle and polarization stability for radar application," *Mater. Res. Exp.*, vol. 5, no. 1, Jan. 2018, Art. no. 15804.

[38] H. Jiang et al., "A conformal metamaterial-based optically transparent microwave absorber with high angular stability," *IEEE Antennas Wireless Propag. Lett.*, vol. 20, no. 8, pp. 1399–1403, Aug. 2021.

[39] X. Lei et al., "Design and analysis of a novel compact metamaterial absorber based on double-layer ITO resistive film for improving signal integrity," *IEEE Access*, vol. 10, pp. 24067–24079, 2022.

[40] J. B. O. de Araujo, G. L. Siqueira, E. Kemptner, M. Weber, C. Junqueira, and M. M. Mosso, "An ultrathin and ultrawideband metamaterial absorber and an equivalent-circuit parameter retrieval method," *IEEE Trans. Antennas Propag.*, vol. 68, no. 5, pp. 3739–3746, May 2020.